Intercomparison of NO_2 Concentrations between Point Measurements and Long Path Measurements

By: Yosra Maher

Supervisor: Dr. McLaren

Committee member 1: Dr. Hastie

Committee member 2: Dr. Rudolph

Course director: Dr. Wilson

Abstract

Measurements of NO_2 were collected using Active-Differential Optical Absorption Spectroscopy (DOAS). An intercomparison between DOAS and chemiluminescence was completed. Data sets presenting the intercomparison between the two methods are presented for February 22-23, 2016, February 26-27 2016, March 4-5 2016 and March 21-22 2016. The intercomparisons are accompanied by meteorology factors wind speed and delta T as well as concentrations of O_3 for one stable night and one unstable night. The data sets illustrated that the DOAS instrument measuring concentration of NO_2 over a long path length does in fact provide an accurate representation of the concentration of NO_2 at single point measurements. There were slight deviations between the two instruments that could primarily be accounted for by spatial averaging and meteorology effects. Chemical factors were also observed to deviate DOAS measurements from chemiluminescence, however this is seen more often during unstable nights when other NO_y such as HONO, N_2O_5, NO_3 and HNO_3 interfere with the chemiluminescence instrument.

Acknowledgments

I would like to express my sincerest gratitude to Professor Robert McLaren. His timely wisdom, constant guidance, understanding and availability paved the way to my successful completion of this research project. My most heartfelt appreciation goes out to Dr. Robert McLaren's graduate students Zoe Davis and William Fujs for their continuous support throughout this project. I would also like to thank Dr. Rudolph and Dr. Hastie for giving up their valuable time to be a part of my committee. Lastly I would like to thank the Center for Atmospheric Chemistry at York University for providing me with the equipment and space to complete this project and Carol Weldon for ensuring all administrative tasks were managed and taken care of.

Table of content

1. Introduction

1.1 Summary of earth's atmosphere

Understanding the atmosphere and its constituents has great significance to protecting physical and biological life on earth. Earth only encompasses a fraction of the atmosphere. The earth's atmosphere is composed of a thin layer of many trace gases, some of which include, NO_2, SO_2, NO_3, CO and HONO. (Yilmaz, 2012). It is vital to human health to understand the sources and reactions of these trace gases. Earth's atmosphere contains 5 major layers that include the following from highest to lowest: exosphere, thermosphere, mesosphere, stratosphere and troposphere.

The troposphere extends vertically 12 km up from the surface of the earth (Barry, 1971) . Most major air pollutants are in the troposphere; measurements of trace gases in this thesis pertain to this region of the atmosphere. A major factor that dictates the structure of the atmosphere is its temperature profile. The troposphere is capped by a temperature inversion at the tropopause, which consists of a warm layer residing on a cooler layer(Barry, 1971). This is titled a temperature inversion because the warmer air is located underneath the cooler air so often times the temperature declines at increasing altitude because heat is transferred often from earth's surface. The area closest to the surface of the earth is known as the planetary boundary layer, PBL(Wojtal, 2013). A schematic of the diurnal variations and dynamics of the PBL is shown below:

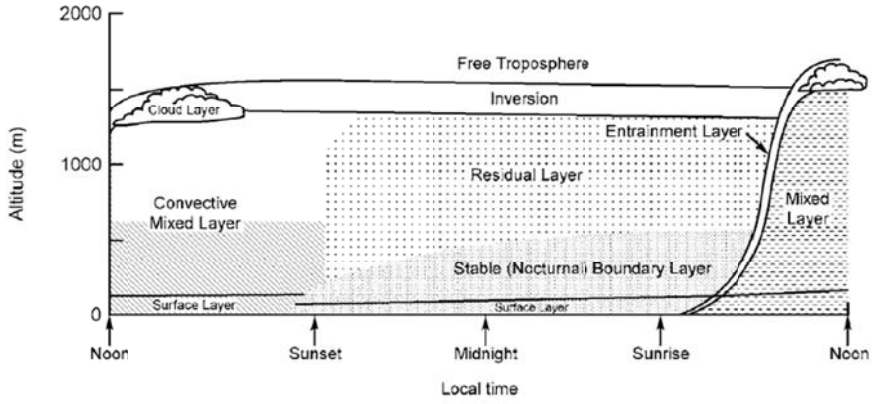

Figure 1: Diurnal variation and dynamics of the planetary boundary layer (PBL).Taken from Stull, 1988.

During the daytime, there is greater mixing in the PBL due to atmospheric turbulence driven by wind shear and convection. The turbulence originates from the diurnal variance of solar radiation (Wojtal, 2013). During the night, radiative cooling leading to the reduction of convection lead and as a result reducing in the mixing occurring in the PBL. Within the troposphere, almost all of earth water vapor and moisture resides which is the major cause of earth's weather.

Air pollution has become a serious climatic concern in this day in age. It occurs in the atmospheric boundary surrounding the earth. Air pollution and meteorological effects are heavily intertwined. These effects include wind speed, wind direction, wind velocity, temperature and humidity. Understanding effects of meteorology is important because it assists in the dispersion, transformation and removal of air pollutants from pollution source regions in the atmosphere(Ocak and Turalioglu, 2008). Air pollutants such as NO are emitted from the earth directly to the atmosphere through combustion reactions between N_2 and O_2. These pollutants are classified as primary pollutants and derive from all types of fossil fuel combustion such as traffic and industrial emissions (Ocak and Turalioglu,2008). A second type of pollutants is classified as secondary

pollutants. These originate from chemical reactions transforming one reactant into another. Ozone is a classic example of a secondary pollutant since there are no known primary sources.

1.2 Chemistry of nitrogen in the atmosphere

Nitrogen species are categorized as either NO_x or NO_y species. NO_x species are the sum of NO and NO_2. These two gases are constantly interconverting in the presence of light and are therefore classified in one group. NO_y species include nitrogen species in the atmosphere such as HONO, HNO_3, N_2O_5, NO_3, etc. species are abundant throughout the lower atmosphere and as a result they heavily impact the chemistry of the atmosphere (Platt and Stutz, 2008). They originate primarily from anthropogenic combustion emissions from traffic and industrial combustion sources, which are located at the earth's surface. N_2 reacts with O_2 in the air to form NO and NO_2 gas.

$$N_2 + O_2 \rightarrow 2NO^{\cdot} \quad \text{(R.1)}$$

$$N_2 + 2O_2 \rightarrow 2NO_2^{\cdot} \quad \text{(R.2)}$$

Under photolysis, NO_2 can then transform to NO at wavelengths lower than 420nm.

$$NO_2 + hv \rightarrow NO + O(^3P) \quad \text{(R.3)}$$

$O(^3P)$ is converted to ozone, O_3, through its reaction with O_2

$$O(^3P) + O_2 \rightarrow O_3 \quad \text{(R.4)}$$

NO_2 is then formed through the rapid reaction between O_3 and NO_2.

$$NO^{\cdot} + O_3 \rightarrow NO_2^{\cdot} + O_2 \quad \text{(R.5)}$$

Through the reaction of NO_2 and O_3 in the atmosphere at night, NO_3 is formed. This reaction is temperature independent and is only seen when temperature rises above 0°C (Platt and Stutz,

2008). NO_3 is detected between 580-670nm due to its absorption in the red region. NO_3 has a lifetime of 5 seconds during the day and under photolysis NO_3 dissipates into the following (patryk➔ wayne). At night the lifetime of NO_3 is typically 1-3 minutes (McLaren et al., 2010):

$$NO_3 + hv \rightarrow NO_2^{\cdot} + O(^3P) \quad \text{(R.6)}$$

$$\rightarrow NO^{\cdot} + O_2 \quad \text{(R.7)}$$

Quantifying concentrations of NO_2 and NO_3 allow for the further analysis of N_2O_5, which has yet to be measured directly on its own. However, significant amounts of NO_3 are needed to estimate the concentration of N_2O_5. N_2O_5 is stabilized at colder temperatures (patryk).

$$NO_3^{\cdot} + NO_2^{\cdot} \leftrightarrow N_2O_5 \quad \text{(R.8)}$$

N_2O_5 is also significant because it is involved in the removal process of nitrogen species from the atmosphere. It is hydrolyzed to form HNO_3 under both heterogeneous and possibly homogenous channels. HNO_3 is removed from the atmosphere through wet and dry deposition. Hydrolysis under heterogeneous channel is presented below:

$$N_2O_5 + H_2O_{(p)} \rightarrow 2HNO_{3\,(p.g)} \quad \text{(R.9)}$$

Hydrolysis under homogenous channel is presented below:

$$N_2O_5 + H_2O_{(g)} \rightarrow 2HNO_{3\,(g)} \quad \text{(R.10)}$$

1.3 Differential optical absorption spectroscopy

In order to quantify the concentration of trace gases in the atmosphere, differential optical absorption spectroscopy (DOAS) is employed. It allows for the unambiguous identification of trace causes by measuring the change in light intensity that occurs in the atmosphere as a result of these gases. DOAS is non-invasive which renders this method useful for detecting concentrations

of reactive trace gases. DOAS ignores smooth broadband extinction features while measuring the narrowband absorptions. Some examples of smooth broadband extinction features include Rayleigh scattering and aerosol scattering.

DOAS techniques can further be divided into passive and active DOAS techniques. Passive DOAS utilizes natural light sources like sunlight, moonlight and even stars. Active DOAS techniques on the other hand use artificial light sources. Active DOAS is effective in measuring the concentration of trace gases in the lower troposphere. The work presented utilized Active DOAS, which consists of a telescope transmitting light from an artificial light source over a known path length.

1.4 Theory of differential optical absorption spectroscopy

The principle of operation of DOAS is founded on the Beer-Lambert's law (Plane and Smith, 1995):

$$I(\lambda)=I_0(\lambda)e^{-\sigma(\lambda)Lc} \tag{E.1}$$

where $I_0(\lambda)$ is the wavelength dependent intensity, $I(\lambda, L)$ is the remaining intensity, L is the light path length in the material and $\sigma(\lambda)$ is the wavelength absorption cross section of the molecule. The optical density, D, of a given species is given by:

$$D=\ln\frac{I_0(\lambda)}{I(\lambda)}=\sigma(\lambda)Lc \tag{E.2}$$

The optical density is the attenuation in light intensity as a result of the medium it encompasses. Rearranging this equation gives the concentration of trace gases:

$$C=\frac{D}{\sigma(\lambda)L}=\ln(\frac{I_0(\lambda)}{I(\lambda)})(\sigma(\lambda)L)^{-1} \tag{E.3}$$

When quantifying concentrations of trace gases, it is important to account for the presence of stray light as a result of using an open path. Rayleigh and Mie scattering are sources of stray

light that must be accounted for. Mie scattering occurs as a result of aerosol particles in the atmosphere. Rayleigh scattering arises from light travelling though the air, giving rise to photon scattering. Rayleigh scatting is inversely proportional to the fourth power of the wavelength. To account for Rayleigh scattering, the Rayleigh extinction coefficient, $\epsilon_R(\lambda)$, must be presented:

$$\epsilon_R(\lambda) = \sigma_R(\lambda) n_{air} \tag{E.4}$$

where n_{air} is the air mass factor 2.45 x 10^{19} molecules cm^{-3} at 20° and 1 atm and $\sigma_R(\lambda)$ is 4.4 x 10^{-16} $cm^2 nm^4$.

$$\sigma_R(\lambda) = \sigma_{RO} \lambda^{-4} \tag{E.5}$$

The Mie extinction coefficient, $\epsilon_M(\lambda)$, is defined as:

$$\epsilon_M(\lambda) = \epsilon_{MO} \lambda^{-n} \tag{E.6}$$

Taking Mie scattering and Rayleigh scattering into account extends the Beer Lambert equation to the following:

$$I(\lambda) = I_0(\lambda) e^{L(-\sigma(\lambda)c + \varepsilon R(\lambda) + \varepsilon M(\lambda))} \tag{E.7}$$

This equation can further be expanded to account for the various trace gases present in the atmosphere:

$$I(\lambda) = I_0(\lambda) e^{L(-\Sigma \sigma_i(\lambda) c_i + \varepsilon R(\lambda) + \varepsilon M(\lambda))} \tag{E.8}$$

where i describes the i^{th} absorbing species.

In order to determine the light intensity in the absence of absorbing species, the absorption of cross section of the given gas must be determined which is separated into two components:

$$\sigma_i(\lambda) = \sigma_{i,0}(\lambda) + \sigma_i'(\lambda) \tag{E.9}$$

where $\sigma_{i,0}(\lambda)$ is the slowly varying broadband component with regards to wavelength. $\sigma_i'(\lambda)$ is the rapidly varying narrowband component with regards to wavelength.

Combining the above 2 equations results in:

$$I(\lambda)=I_0(\lambda)e^{-L(\Sigma\sigma'_i(\lambda)c_i)}\, e^{-L(\Sigma_{i0}(\lambda)c_i+\varepsilon_R(\lambda)+\varepsilon_M(\lambda))}\, A(\lambda) \quad \text{(E.10)}$$

Where A (λ) is the attenuation factor describing the broadband transmission of the optical system that is dependent on wavelength.

The differential optical density, D' can be defined as:

$$D' = \log\frac{I'_0(\lambda)}{I(\lambda)} = L\Sigma(\sigma'_i(\lambda)c_i) \quad \text{(E.11)}$$

and the concentration of the absorbent *i* is defined as:

$$C_i = \frac{D'}{\sigma'_i(\lambda)L} \quad \text{(E.12)}$$

Using the equation above plus the long equation to measure the intensity of light together measure the concentration of trace gases in the atmosphere.

Purpose of project:

The objective of this thesis is to determine how accurate long path measurements of NO_2 mixing ratios by the DOAS instrument are to point measurements taken by the chemiluminescence instrument. The goal is to determine the difference between the two methods mathematically so that NO_2 mixing ratios can be accurately identified.

2. Experimental

2.1 Data Collection

Measurements of NO_2 were taken from October 2015 to March 2016 at York University using an Active DOAS system comprised of a modified DOAS 2000 instrument (figure 2.2). Within the instrument is a telescope capable of transmitting and receiving light. Since this is an Active DOAS system, it must include an artificial light source. A 150W Xenon-arc lamp. This lamp is located in front of the primary telescope mirror. The beam is transmitted through an open path onto a retro-reflector composed of 7 x 2" corner cubes located roughly 1 km away from the Petrie Science building. The transmitted beam is reflected back on to the telescope, where it is focused on to a single 600 μm quartz fiber optic cable, creating a total path length of 2.2 km.

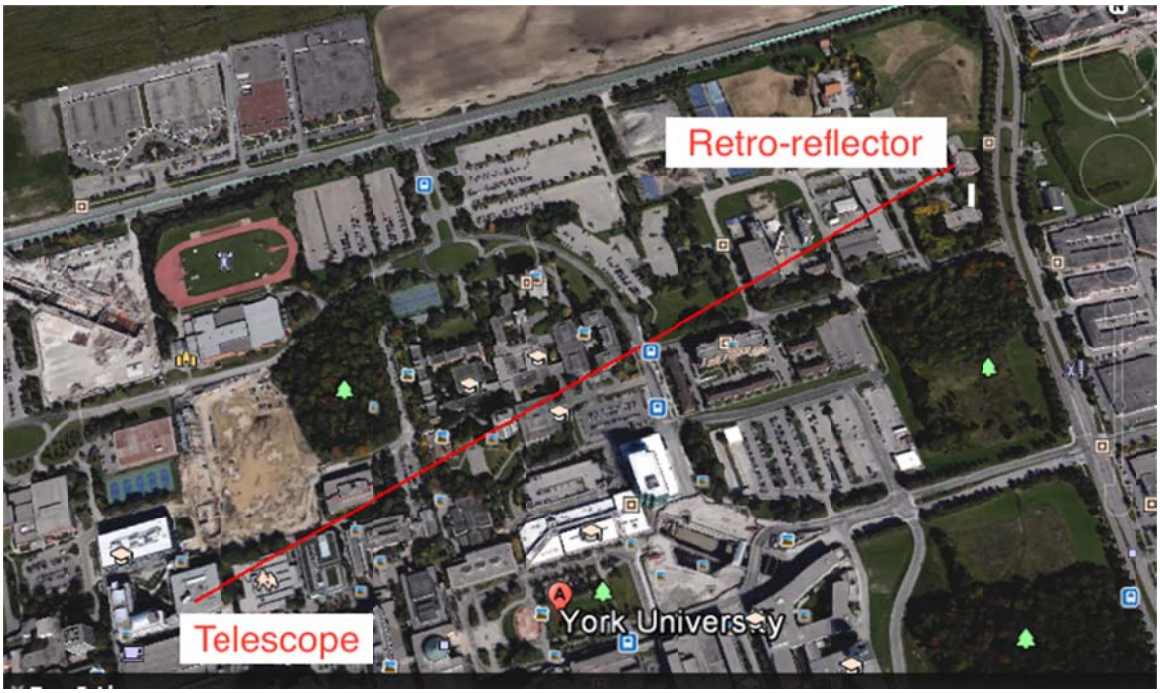

Figure 2.1: Path length from DOAS 2000 instrument to the retro-reflector where light is transmitted and reflected back on to the instrument.

The DOAS 2000 instrument is connected to a spectrometer, S2000, which allows for the collection of trace gases between the wavelengths 500nm-800nm. A red spectrometer detecting this large range is used because it allows for the identification of both NO_2 and NO_3. Although the typical range to measure NO_2 is not 500-800nm but rather 450nm, it was used for the advantage of simultaneously measuring NO_2 and NO_3, allowing for better determination of N_2O_5. Despite this, the current project was not focused on determination of NO_3 and N_2O_5. This spectrometer is connected to a computer that controls the spectrometer using OOIBase 32 software.

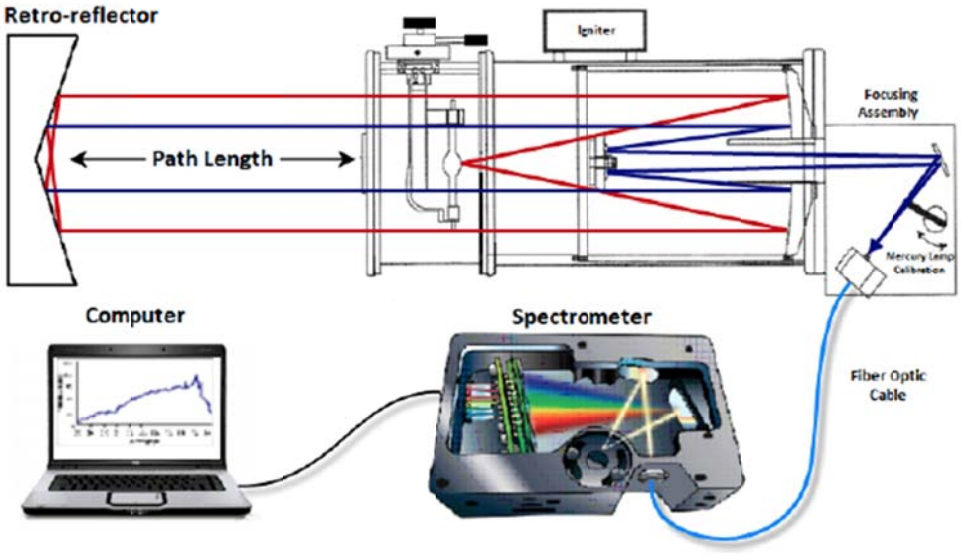

Figure 2.2: Experimental set up used to measure concentration of trace gases in the atmosphere.

In order to accurately measure the concentration of trace gases, the spectrometer wavelength range must first be calibrated so that corrections can be applied to gas spectra. This is done by collecting spectra for offset, dark current, xenon-arc lamp, mercury lamp and a helium neon laser. These calibration spectra must be collected at the same temperature as the sample spectra.

An Offset spectra is collected at an integration time of 7 ms over 30000 averages and consists of a positive baseline independent of light. For this reason, offset collections must be completed in the absence of light.

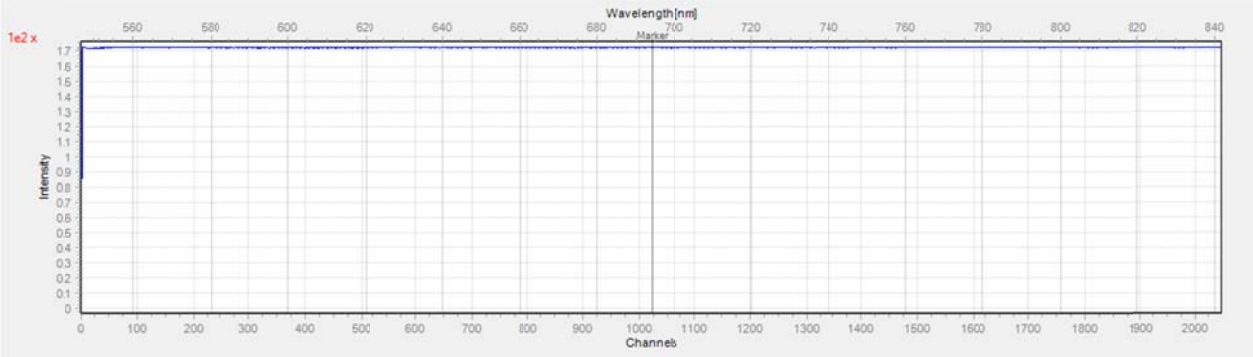

Figure 2.3: Sample spectra of offset collected at 7ms over 30000 averages used for spectra correction.

Dark current is collected at an integration time of 15000ms over 30 averages. It provides the instrument's response in the absence of light. The noise in this spectra originates from thermal noise and as a result is proportional to the temperature of the system and the integration time of the spectrometer. A method for decreasing the effect of dark current is to decrease the temperature of the instrument.

$$V_{rms}=\sqrt{4kTR\Delta f}$$

where k is Boltzmann's constant (1.38054×10^{-23} JK^{-1}), T is temperature (K), R is resistance (ohms) and Δf is the frequency bandwidth (Hz).

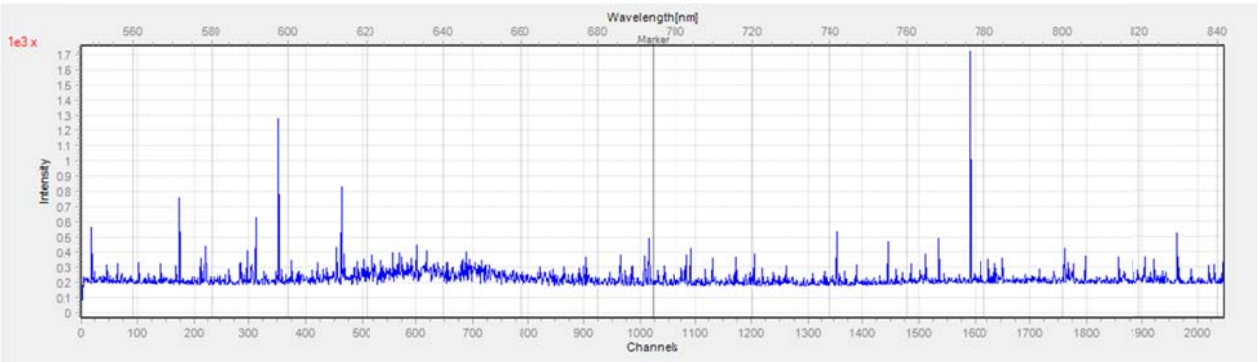

Figure 2.4: Sample spectra for dark current collected at 15000ms over 30 averages, used for spectral corrections.

The mercury lamp along with a helium neon laser source (632.8nm) is collected at an integration time of 7 ms over 30000 averages. It is used for calibration of the wavelength range of the spectra and for convolution of the reference spectra. The spectra are collected by focusing the fiber optic on to the mercury lamp and laser light while blocking any other light source.

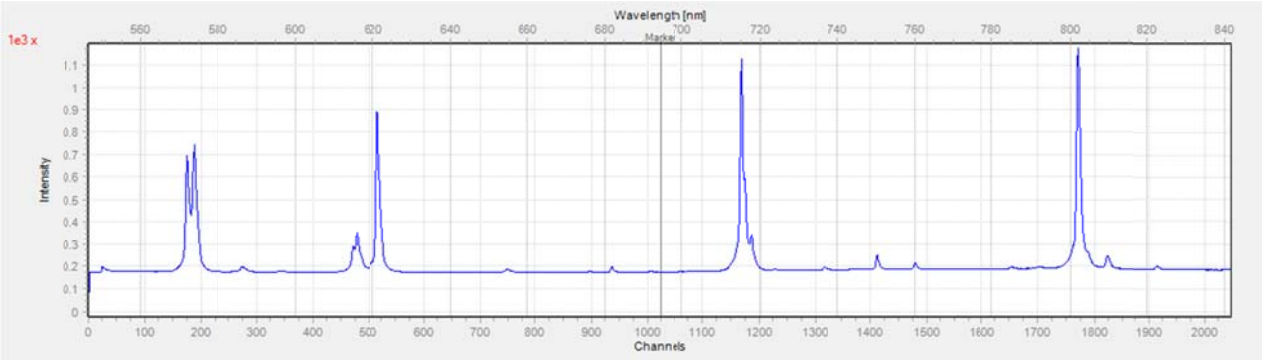

Figure 2.5: Sample spectra for Hg/HeNe collected at 7ms over 30000 averages used to calibrate data.

The xenon-arc lamp is collected at an integration time of 7ms over 30000 averages. However, during some nights, it was collected using an integration time of 9 ms. The principle of operation of this lamp is based on the ionization of xenon gas caused by a high voltage generated when a light arc is produced between the anode and cathode. The telescope emits a light beam when a short arc length is produced between the anode and cathode. The xenon-arc lamp was collected using two methods. The first method consisted of focusing the fiber optic onto the transmitted light from the telescope before it entered the open path of the atmosphere. The second method involved focusing the fiber optic on to the reflected light behind the primary telescope mirror.

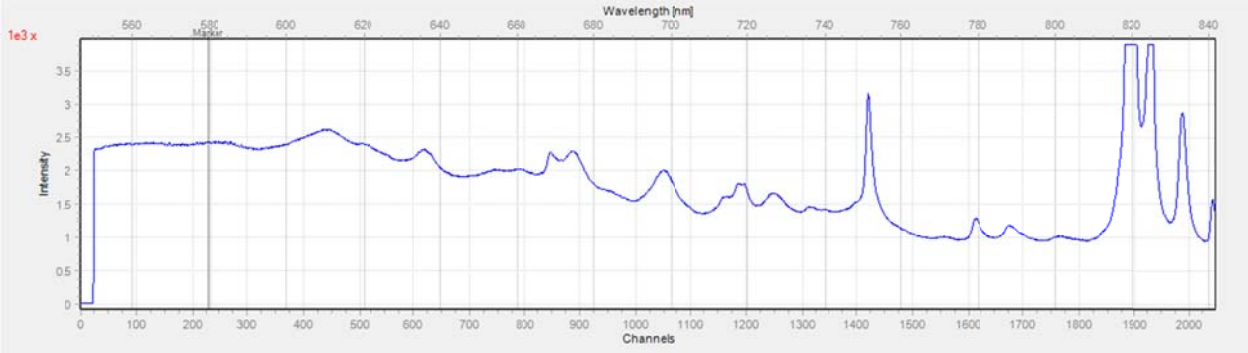

Figure 2.6: Sample lamp spectra collected from the reflected light of the telescope at 9ms over 30000 averages and used to incorporate into fit scenarios.

The last component of the instrumental set up is the mode mixer. The mode mixer bends the fiber optic cable allowing homogenous illumination of the detector that in return, removes redundant spectral structures.

2.2 Spectral/polynomial fitting

Once the calibration spectra as well as the sample spectra are obtained, they must be fitted with the DOASIS software. First, the mercury lamp, helium neon laser, xenon arc lamp and the sample spectra are corrected for offset and dark current by subtracting them from the corresponding spectra. Next, the wavelength calibration is corrected for the mercury lamp and helium neon laser. The wavelength calibration was performed using wavelengths 576.96 nm, 579.07 nm and 632.8 nm. The calibration function was performed using a 2^{nd} order polynomial. The Gaussian fit was created using the helium neon laser wavelength absorption at 632.8 nm. Before the fit scenario could be created, the spectrometer's spectra must match the resolution of the reference spectra through a process called convolution. The resolution of the spectrometer is taken from the Gaussian fit created from the helium neon laser at 632.8 nm. Upon performing wavelength calibrations and convoluting high-resolution reference spectra, conditions for a fit

scenario could then be specified. First, the fitting range specific to the gas under study must be set. A fitting range of 560-585nm is used for NO_2 analysis. H_2O and O_4 cross sections are included in this scenario because they show characteristic absorption features that must be accounted for within the range selected. The range is selected in a featureless region in the lamp spectra. The logarithm of the sample spectra is then taken and a 3^{rd} polynomial order is merged into the fit. A 2^{nd} polynomial order is used to account for Rayleigh scattering, Mie scattering and instrumental response features that could potentially affect the accuracy of the fit.

2.3 Chemiluminescence measurements

Point measurements of NO_2 were collected using a chemiluminescence instrument located on top of the Petrie Science and Engineering building at York University. The principle of operation of the chemiluminescence instrument is based on the emission of light from chemical reactions. Emission, like fluorescence, originates from singlet energy levels; they only differ in that the source of emission is from chemical reactions rather than absorption of photons. The instrument consists of an O_3 generator, a reaction chamber, a pump and a photomultiplier tube detector. Only direct measurements of NO can be taken by chemiluminescence. However, the instrument generates O_3 that can react with other nitrogen species, in the reaction chamber, like NO_2 to form NO that is then detected by the PMT. NO_2 mixing ratios were collected every minute.

3. Results and discussion

Following the description of the NO_2 fitting procedure, the mixing ratios of NO_2 measured by the DOAS instrument and the chemiluminescence instrument are presented below along with the concentrations of O_3 for one stable night and one unstable night. The results will be analyzed using meteorology (wind speed and delta T). The intercomparison of the two instruments will be analyzed and discussed.

3.1 NO2 fitting procedure

The concentration of NO_2 was obtained as explained in the experimental section using DOAS 2000 instrument. NO_2 was fit in the range 560-585nm using a red spectrometer. However, this is not the common range used for NO_2 collections. NO_2 gas is commonly fit in the region of 422-450nm (Halla et al, 2011). A red spectrometer collecting the range 500-800nm allows for the detection of both NO_2 and NO_3, together these trace gases can be used to also quantify the concentration of N_2O_5.

The fitting scenario for NO_2 included two lamp spectra; one collected from the same evening and the second collected the following morning. Evidence showed NO_2 was fit more effectively in the presence of two lamps due to the true lamp spectra being bracketed within the two collected spectra. The fit scenario also included cross sections of NO_2 (Vandaele 1997), H_2O (Coheur 2002) and O_4 (Hermans 1999). The calibrated data of the mercury lamp, helium neon laser, offset and dark current noise were also incorporated into the fit. In order to obtain the mixing ratio of NO_2, the slant column density provided by DOASIS must be divided by the path length and air mass factor first.

The following figure represents the fit scenario created on March 21, 2016.

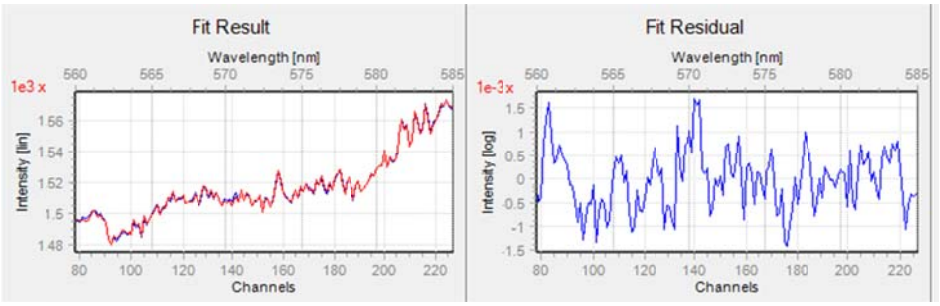

Figure 3.1.1: Fit result and fit residual in the fit scenario created on March 4, 2016.

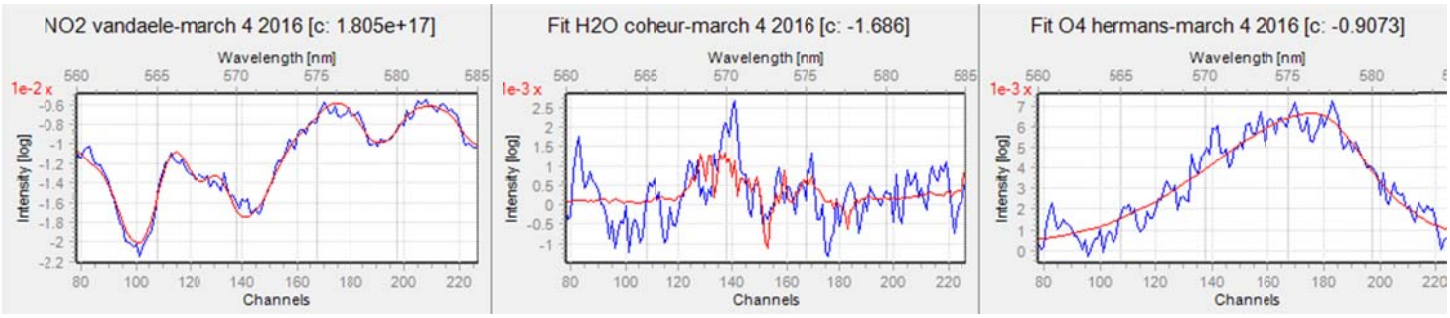

Figure 3.1.2: NO_2, H_2O and O_4 fit results in the fit scenario created on March 4, 2016. During this fit, the mixing ratio of NO_2 is 32.95 ± 0.967ppb.

3.2 Summary of results

Table 3.2.1: Summary of intercomparison between DOAS and chemiluminescence

Date	**Slope**	**Slope error**	**Intercept**	**R^2**
February 22/23 2016	0.864	0.146	0	0.328
February 26/27 2016	0.866	0.113	0	0.351
March 4/5 2016	0.693	0.0891	-1.56	0.841
March 21/22 2016	0.996	0.0196	8.53	0.869

Table 3.2.2: Summary of meteorology effects during nights collected

Date	*Wind Speed*			*Delta T*		
	Min	**Max**	**Average**	**Min**	**Max**	**Average**
February 22/23 2016	0.809	3.606	1.718	-1.831	0.989	0.307
February 26/27 2016	1.97	4.89	3.08	-0.68	0.361	0.0889
March 4/5 2016	-2.66	1.18	0.582	0.00	2.58	1.20
March 21/22 2016	0.678	5.49	1.93	-0.408	1.48	0.570

Perfect intercomparisons would give a slope of 1 with an r^2 value also close to 1. However this is unrealistic and unlikely to occur. The slopes, however, are close to 1 indicating that the

DOAS instrument does give relatively accurate measurements of NO_2 in the atmosphere. Some deviations in the r^2 values are a result of time differences between the DOAS and chemiluminescence instrument. The DOAS instrument was set up to a computer that often lagged in time resulting in systematic errors.

The stability of the night can be inferred through meteorology analysis. Stable nights are defined as those with high NO_2 concentrations, low wind speeds and high delta T. Stable nights occur when the air mass cools faster than its surroundings. The air becomes denser and stratified. As a result, vertical mixing in the air decreases. Unstable nights are defined as those with low concentrations of NO_2, high wind speeds and low delta T. Unstable nights occur when air is cooled slower than surroundings.

3.3 NO_2 measurements by DOAS and Chemiluminescence during stable nights

The following data presented in figures 3.3.1 to 3.3.10 represent concentrations of NO_2 during one night in February and two nights in March.

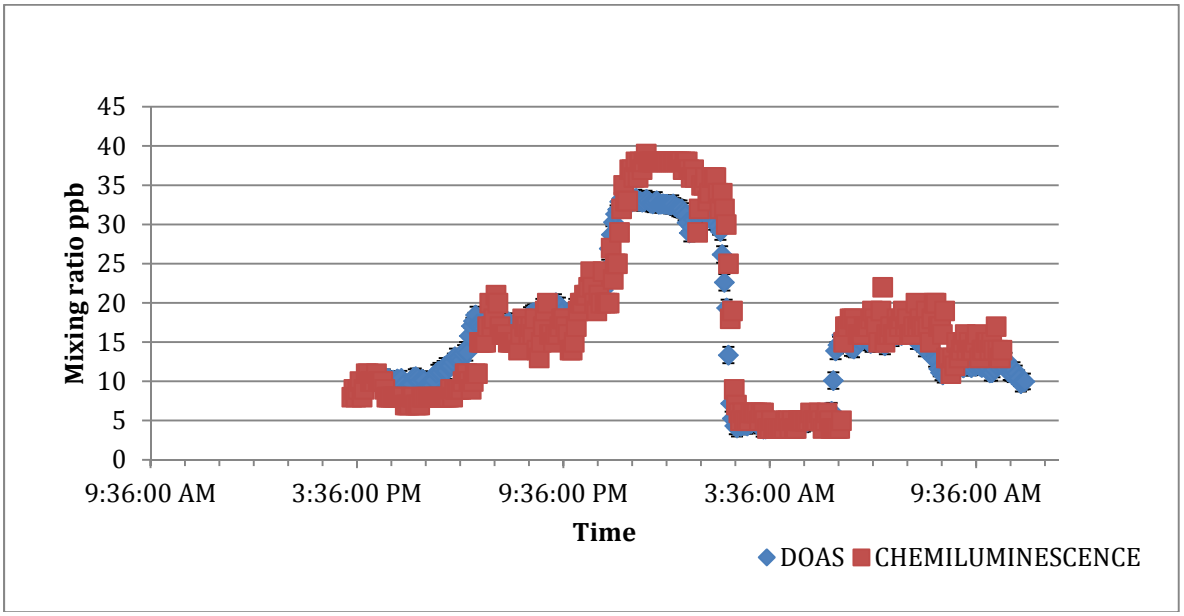

Figure 3.3.1: A plot of mixing ratio vs. time of the concentration of NO_2 measured by both DOAS and chemiluminescence on the night of February 22-23 2016.

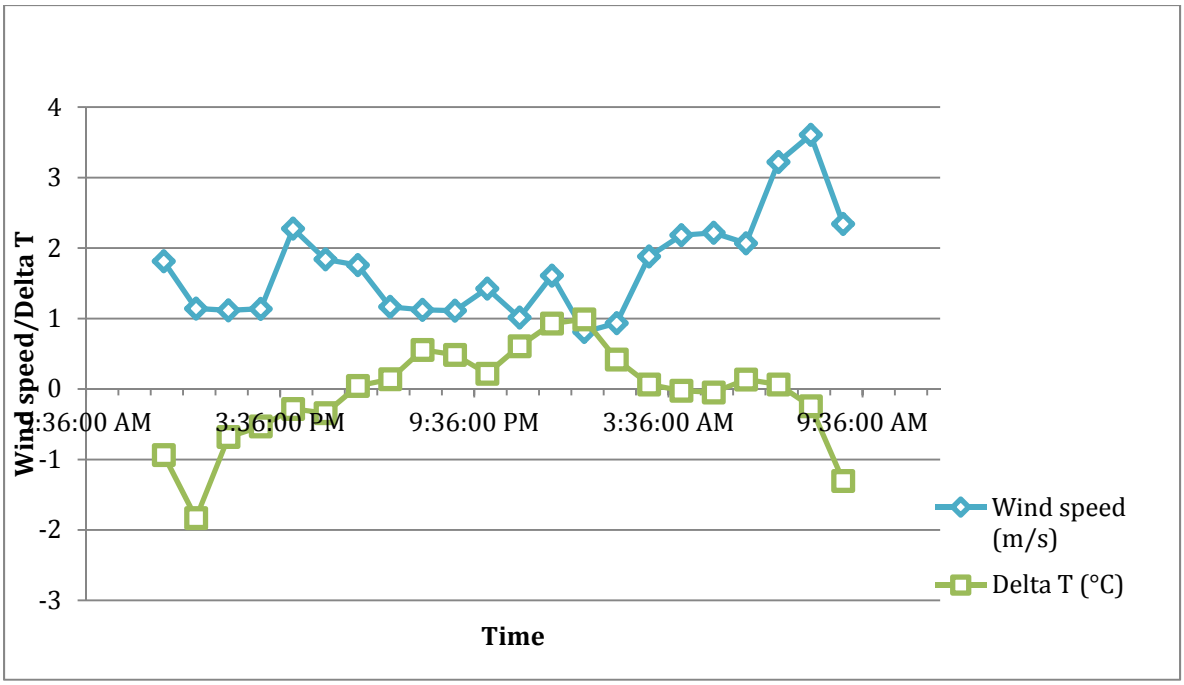

Figure 3.3.2: A plot of windspeed and delta T over time during the night of February 22-23 2016.

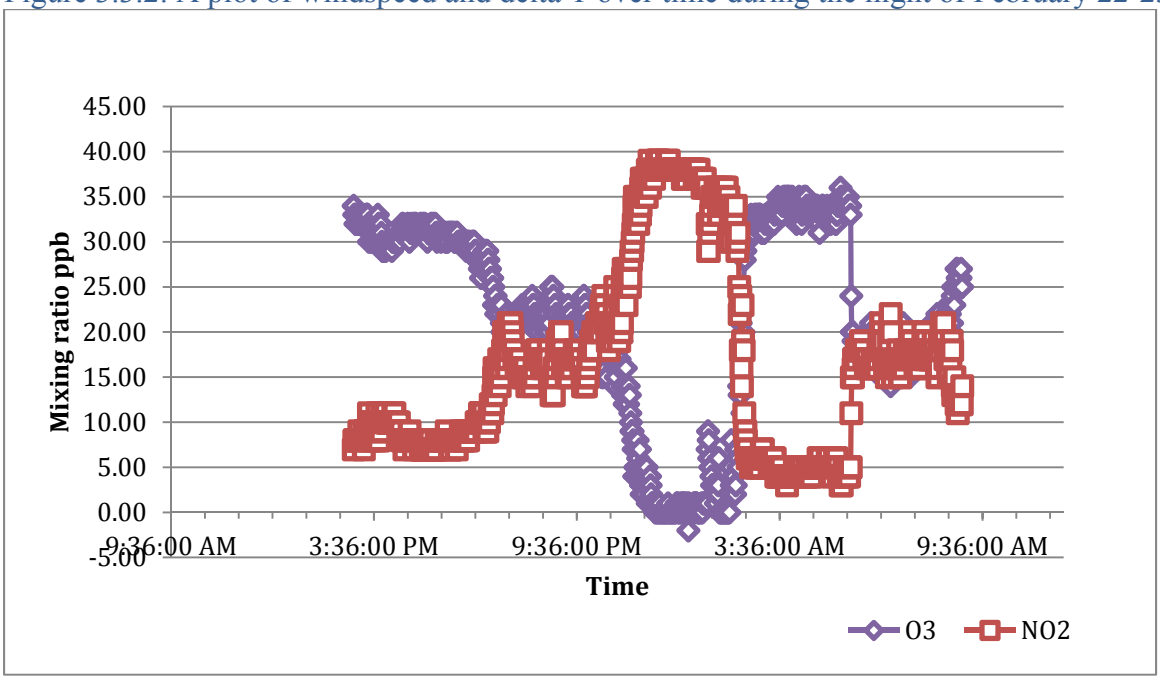

Figure 3.3.3:Comparison between NO_2 and O_3 concentrations in ppb during February 22-23 2016.

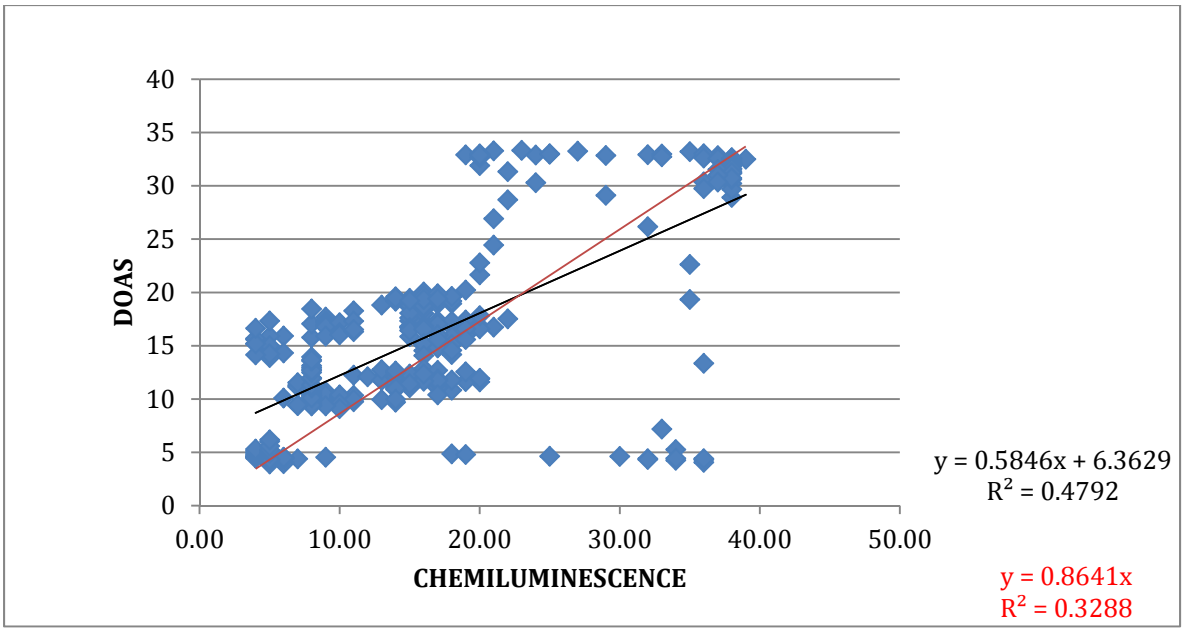

Figure 3.3.4: Intercomparison between DOAS and chemiluminescence instrument on February 22-23 2016.

On this particular night, concentrations of NO_2 rose above 25 ppb indicating the occurrence of a stable night. Looking at table 3.2.2, the average wind speed on this night was 1.718 m/s and the average delta T was 0.31°C. Concentrations of O_3 are expected to drop when NO_2 concentrations increase and vice versa due to the following series of chemical equations:

$$NO_2 + hv \rightarrow NO + O(^3P)$$

$$O(^3P) + O_2 \rightarrow O_3$$

Figure 3.3.3 confirms the interconversion between O_3 and NO_2. Although not shown, a temporal plot of $O_x(O_3 + NO_2)$ shows a roughly constant value all night, emphasizing the role of the "titration" reaction n a stable air mass. The rapid decrease in NO_2 concentrations occurs at approximately 2:00 AM and is due to a change in air mass. At this time, an increase in the wind speed is seen along with a decline in delta T leading to the notion that a change in meteorology is accompanied with rapid changes in NO_2 concentrations. Between 3:00PM and 9:00PM, NO_2 mixing ratios are slightly higher by DOAS versus chemiluminescence with numerous possible

reasons. The chemiluminescence instrument is placed 3-4m higher than the DOAS telescope. A difference in vertical height could affect the concentrations because mixing increases closer to the surface of the earth at the planetary boundary layer. An explanation for this variation could also be the presence of sunlight during this time. Solar radiation was not included in the fit. As a result, there is an over estimation in NO_2 concentrations because of the fraction of the sunlight in the measurements calculated by DOAS. Figure 3.3.5 illustrates the solar radiation present in the residuals at 4: 37 PM. The solar radiation features appear as sharp lines in the residual as seen below.

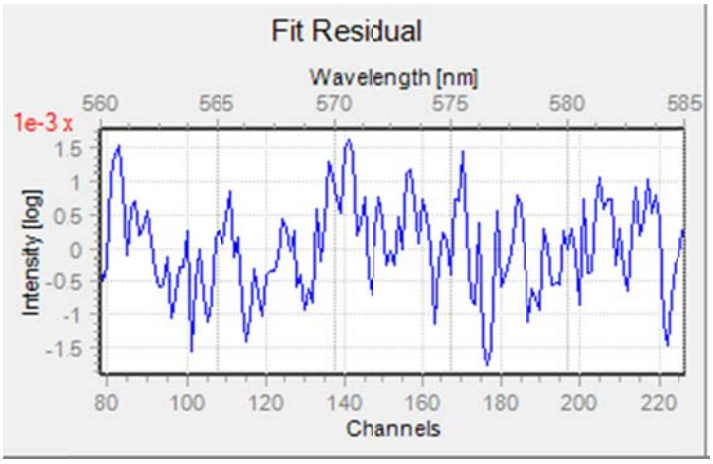

Figure 3.3.5: Fit residuals on February 22, 2016 at 4:37 PM.

Chemically speaking, there are a number of other NO_2 sources in the atmosphere that interfere with the determination of NO_2 measured by the chemiluminescence instrument. The chemiluminescence instrument contains an Mo convertor that reduces oxidized nitrogen species to NO in a flow stream. Apart from NO_2 this interconversion can also occur for oxidized nitrogen species such as N_2O_5, HNO_3, NO_3 and HONO. N_2O_5 could be the biggest contributor of NO_2 at night (estimated1-2 ppb) as it produces two molecules of NO_2 for every molecule of N_2O_5 present. HNO_3 and HONO produce roughly 1 ppb of NO_2 while NO_3 is the smallest contributor of 0.05 ppb (Wojtal et al. 2011). As a result of chemical factors, there could be up to a 5 ppb difference

between DOAS and chemiluminescence methods. On this particular night, this reason cannot explain the entire difference seen since the presence of large NO_2 spikes result from changes in the stability of air mass. N_2O_5 is produced through the chemical reaction between NO_2 and NO_3, which only occur during unstable night as the formation of NO_3 is temperature dependent. Therefore, chemical factors can likely be ruled out as the major reason for disagreement between the two measurement techniques at this time.

The DOAS instrument measures averages of NO_2 mixing ratios over a long path. Spatial and temporal averaging must be considered for this difference in concentration. Spatial averaging is defined as the mathematical mean of values over multiple points in space whereas temporal averaging is defined as the mathematical mean of values over a period of time. A rapid increase in the concentration of NO_2 would result in underestimation of the peak gas concentrations by DOAS. Chemiluminescence measures the concentration of NO_2 at a single point whereas DOAS takes the average over a long path. It is expected that DOAS would not measure rapid spikes in NO_2 that can occur due to local sources.

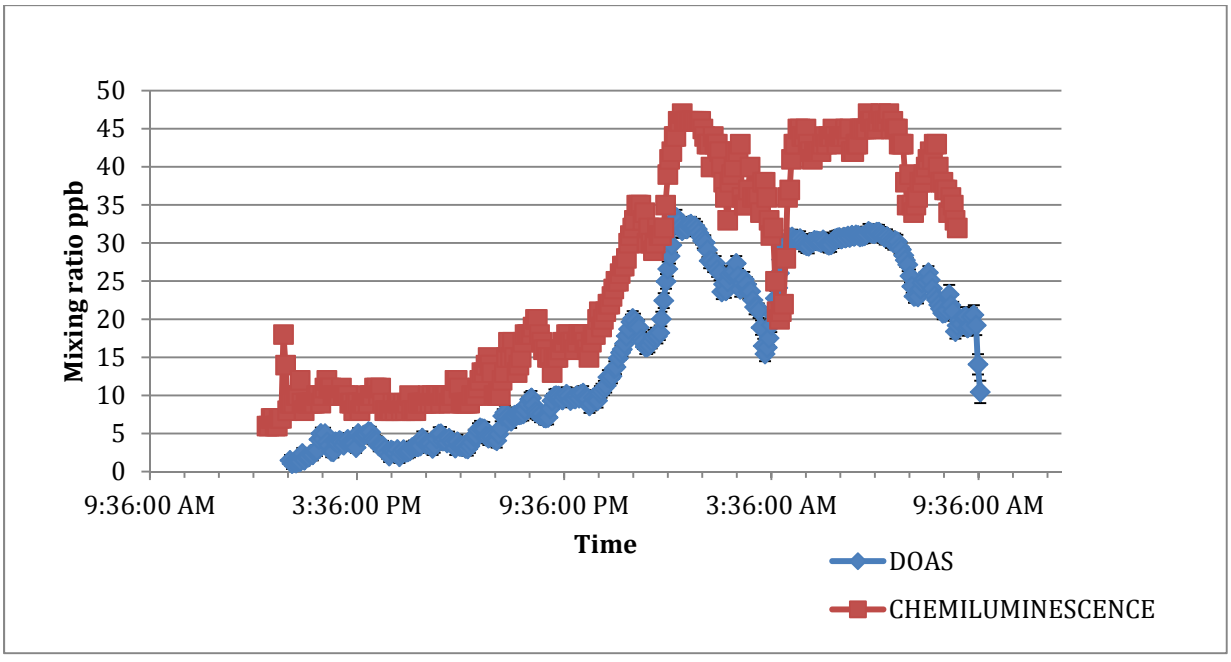

Figure 3.3.6: A plot of mixing ratio vs. time of the concentration of NO_2 measured by both DOAS and chemiluminescence on the night of March 4-5 2016.

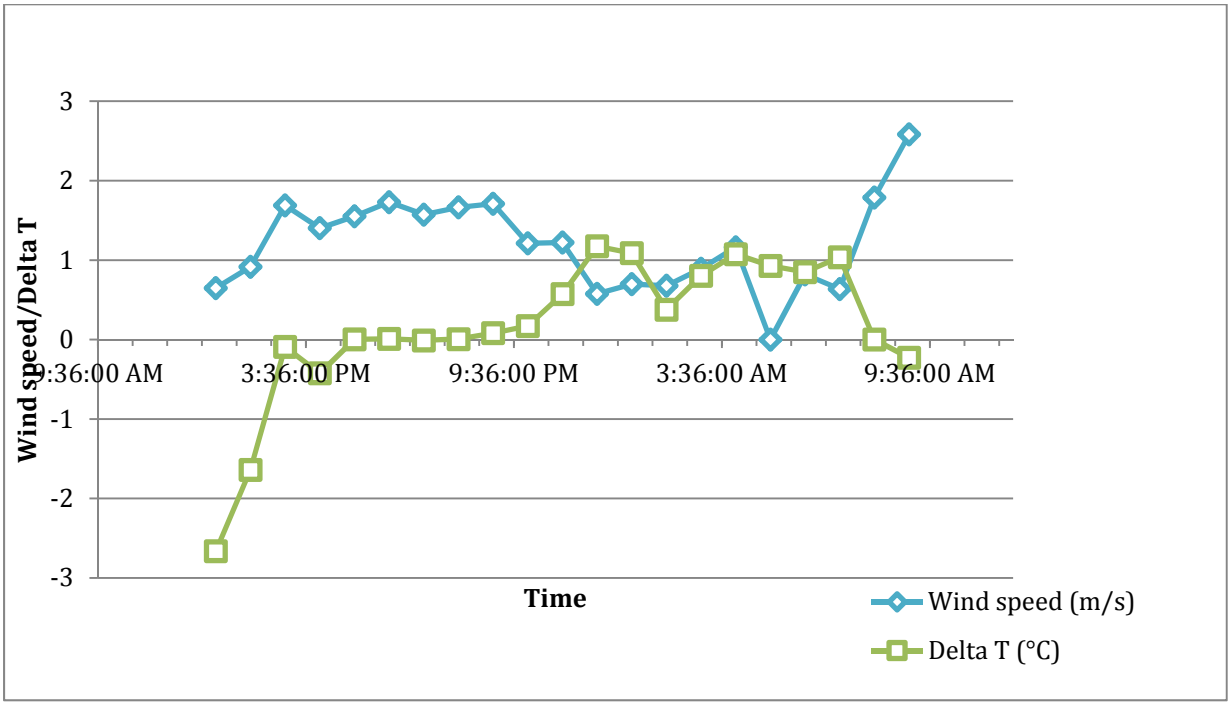

Figure 3.3.7: A plot of windspeed and delta T over time during the night of March 4-5 2016.

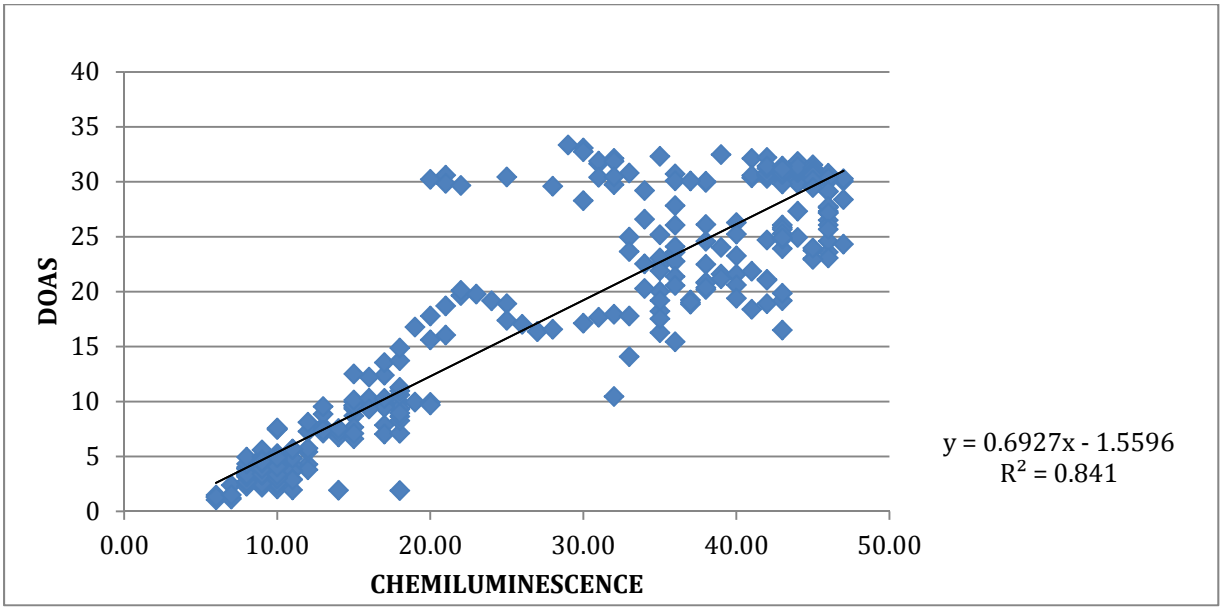

Figure 3.3.8: Intercomparison between DOAS and chemiluminescence instrument on March 4-5 2016.

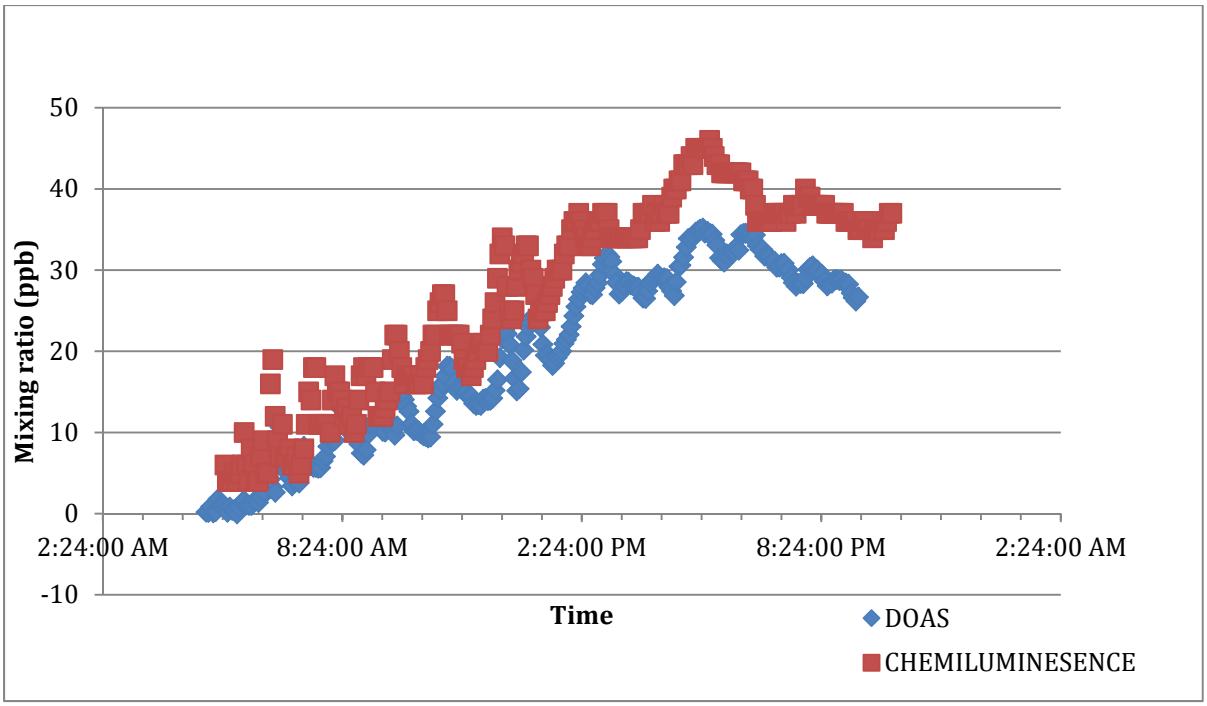

Figure 3.3.9: A plot of mixing ratio vs. time of the concentration of NO_2 measured by both DOAS and chemiluminescence on the night of March 21-22 2016.

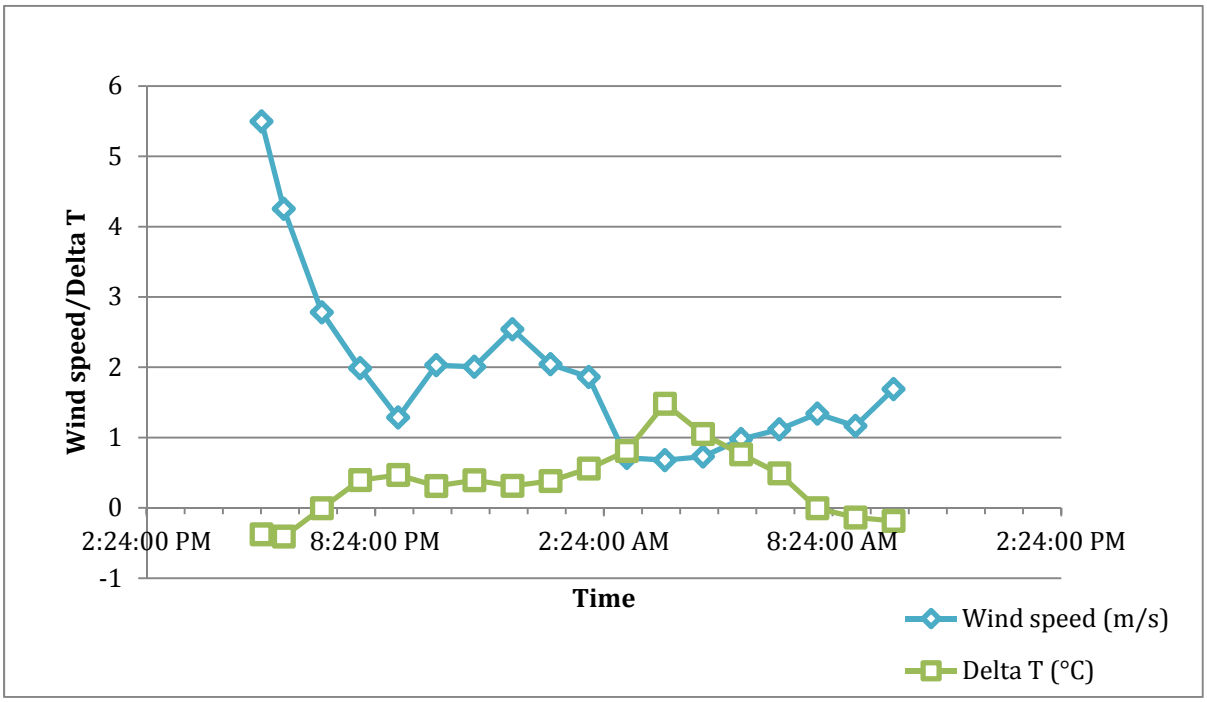

Figure 3.3.10: A plot of windspeed and delta T over time during the night of March 21-22 2016.

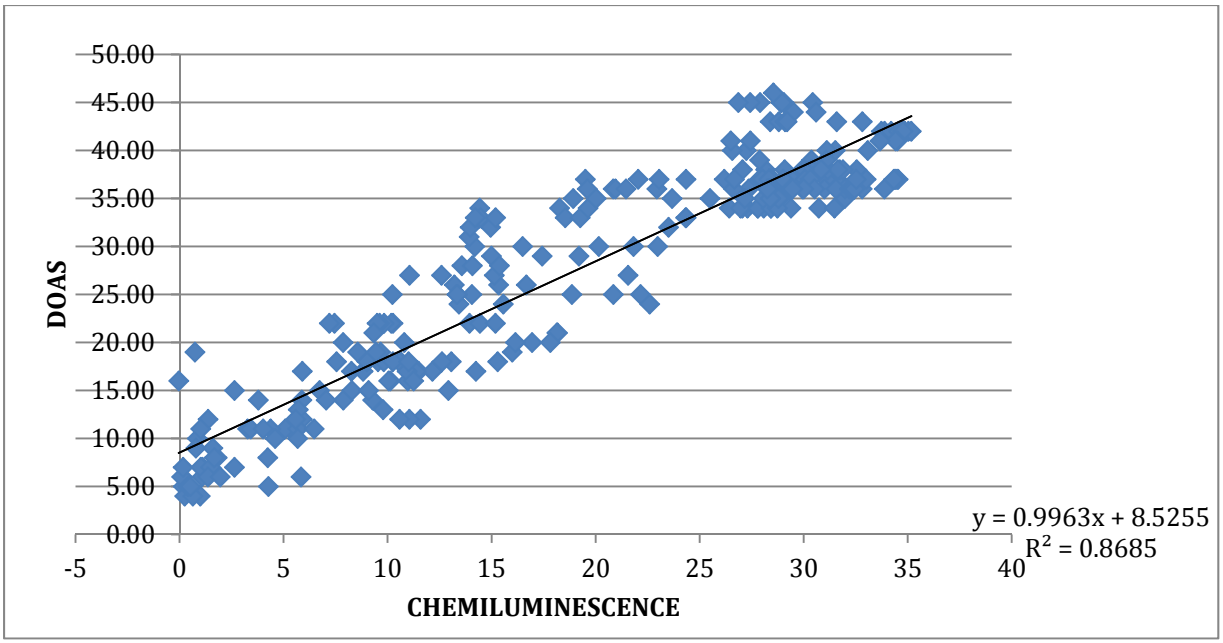

Figure 3.3.11: Intercomparison between DOAS and chemiluminescence instrument on March 21-22 2016.

The DOAS and chemiluminescence instruments differ slightly more during these two nights (figure 3.3.5 to 3.3.10) than in the first night on February 22 2016 (figure 3.3.1-3.3.4). These nights are slightly less stable than February 22, 2016. The average wind speed is lower and the delta T is higher during the two nights in March than in February. Variations in the stability of the night could account for differences in the two methods. It is also observed that the biggest differences between the two instruments occur when there are rapid increases or decreases in the concentration of NO_2, which can be explained by temporal and spatial averages.

3.4 NO_2 measurements by DOAS and Chemiluminescence during unstable nights

The following data (figure 3.4.1 and 3.4.4) represents measurements of NO_2 using a DOAS instrument and a chemiluminescence instrument and their correlation. The meteorology on this night is presented in figure 3.4.2 and the ozone and NO_2 comparison is shown in figure 3.4.3.

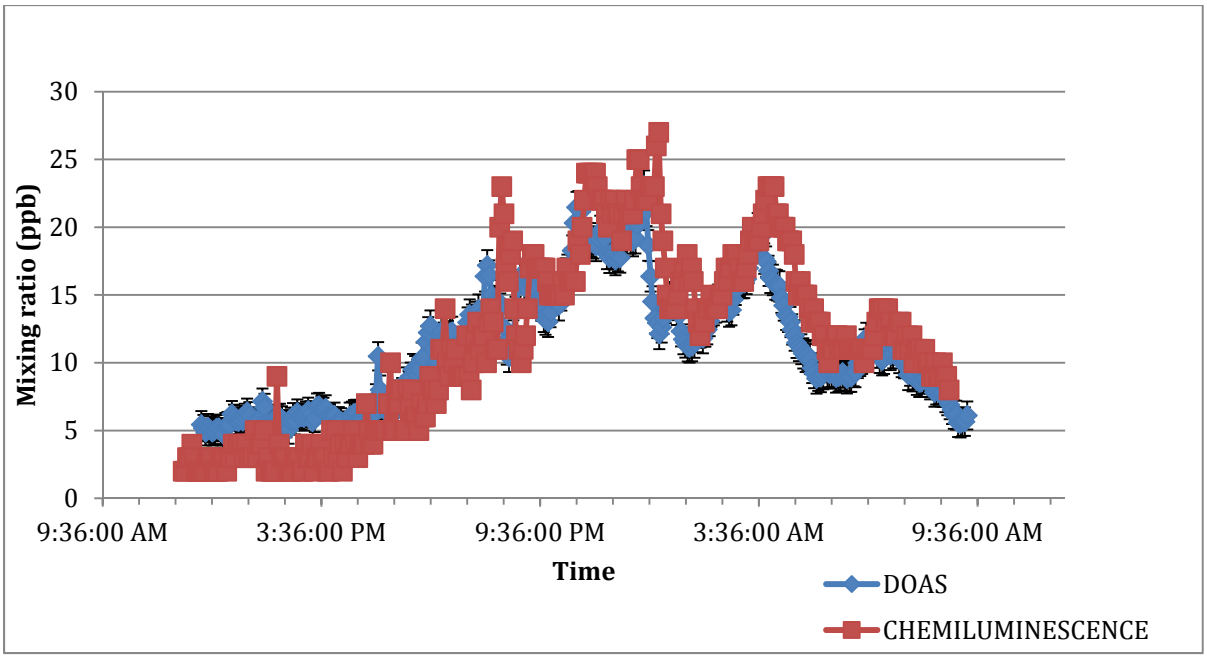

Figure 3.4.1: A plot of mixing ratio vs. time of the concentration of NO_2 measured by both DOAS and chemiluminescence on the night of March February 26-27 2016.

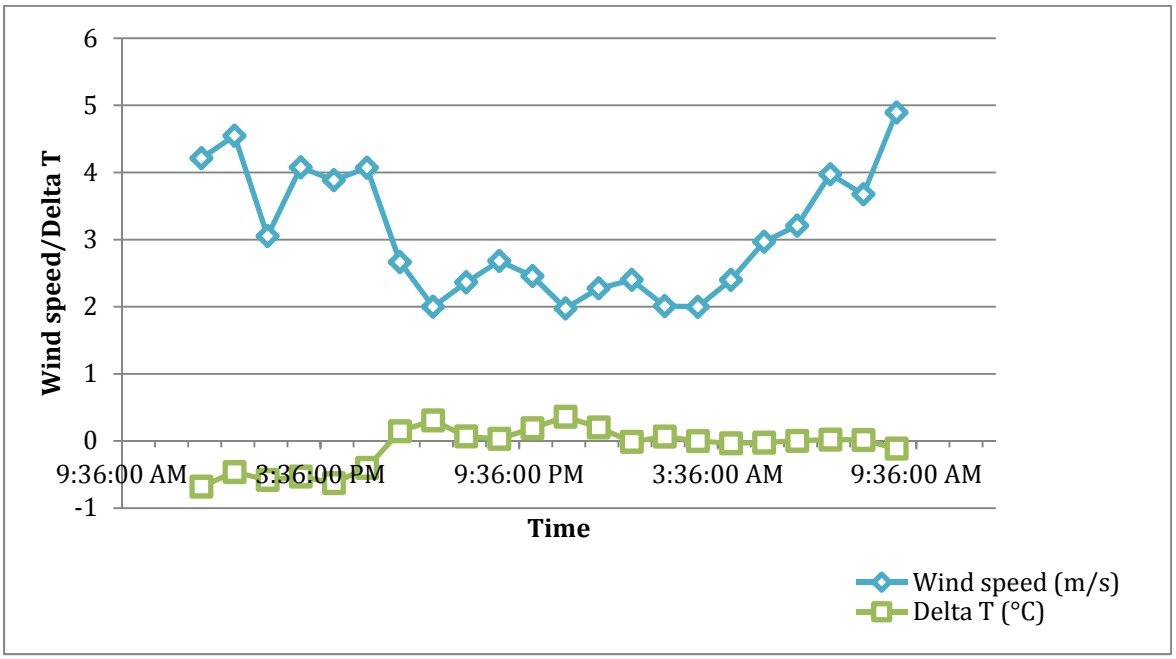

Figure 3.4.2: A plot of windspeed and delta T over time during the night of February 26-27 2016.

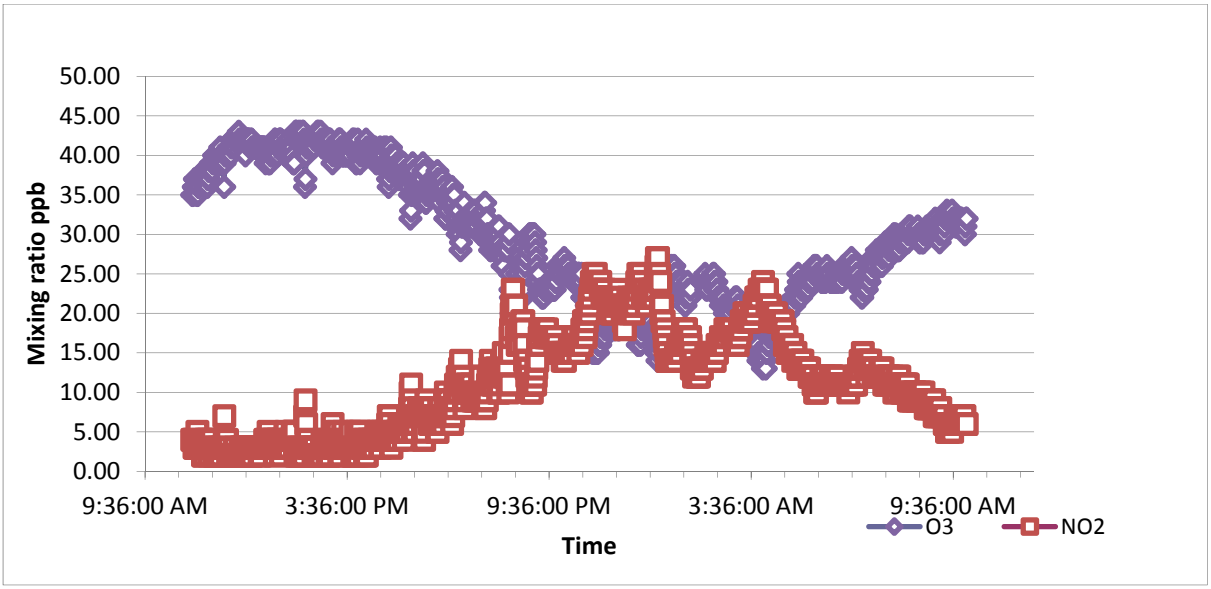

Figure 3.4.3: Comparison between NO_2 and O_3 concentrations in ppb during February 26-27 2016.

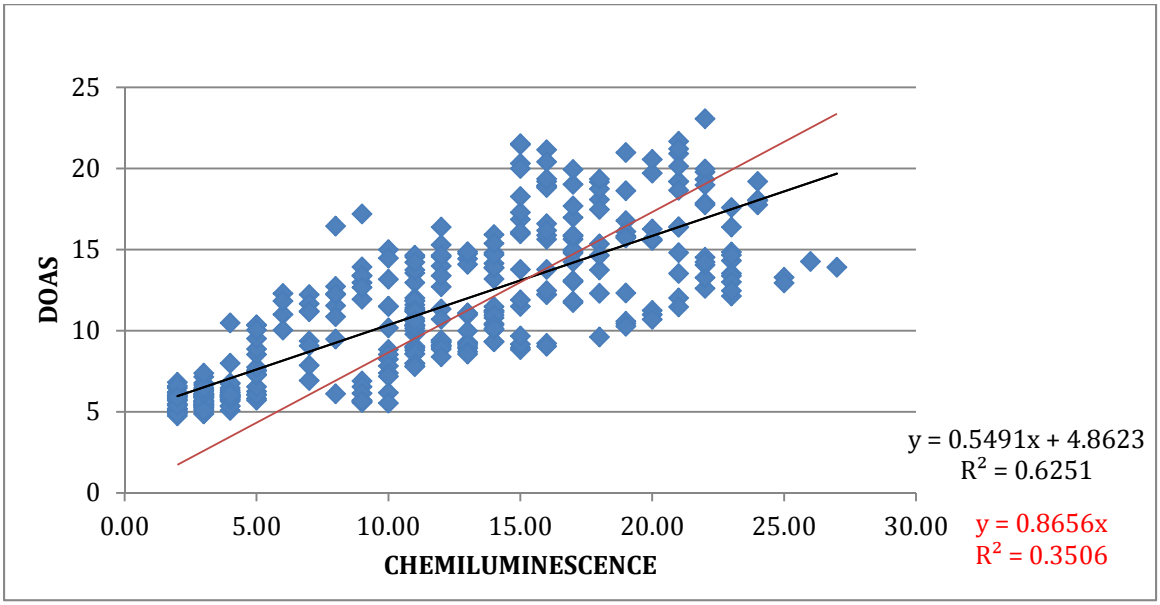

Figure 3.4.4: Intercomparison between DOAS and chemiluminescence instrument on February 26-27 2016.

February 26 2016 (figure 3.4.1 to 3.4.4) is an example of an unstable night. Concentrations of NO_2 do not rise above 25 ppb. Wind speeds on this night are high and delta T values are low indicating the occurrence of an unstable night. Variations in DOAS and chemiluminescence are seen when

concentrations of NO_2 increase or decrease rapidly. It has been observed that changes in stability of the night correspond to differences between the two experimental methods.

Generally speaking, the DOAS instrument is relatively accurate to the chemiluminescence during this unstable night. It is observed again that the concentration of NO_2 measured by the DOAS than chemiluminescence is higher before sunset and lower in the absence of sunlight. This can be explained by the presence of solar radiation that the DOAS instrument collects.

(Insert fit during the day)

Because this is an unstable night, N_2O_5 is likely present and can account for some of the difference in concentration between the two methods. However, N_2O_5 is only present at night and a constant variation between the two methods is observed. Chemical factors explain the larger variations when NO_2 concentrations are spiked. A likely explanation for the differences between the methods is experimental. Because the DOAS instrument produced concentration of NO_2 with little noise, there was likely an error in the fit that resulted in constant underestimations in the concentration of NO_2 throughout the night.

3.5 Error Analysis

The major source of error in the fit procedure is obtaining the real spectra of the lamp. Collecting the lamp spectra using the transmitted light from the telescope showed very poor results. A solution to this problem was to collect lamp spectra using the light reflected from the retro-reflector. However, this still resulted in poor NO_2 fits. Good fits were only obtained when a lamp spectra was collected the following morning indicating that true lamp lied somewhere between the evening lamp and the morning lamp spectra. Another source of error in the fitting procedure was the assumption made when fitting the He/Ne laser at 632.8nm to a Gaussian curve that is only an approximation.

Systematic errors were also present during the experiments. The computer that was used to collect spectra was delayed in time and as a result did not give the exact representation of the atmosphere at that point in time. To resolve this issue, the time of collection by DOAS was adjusted to match the time of collection by the chemiluminescence instrument manually.

4. Conclusion and future work

It is evident that there is a large correlation between the DOAS instrument and the chemiluminescence instrument used to measure the mixing ratio of NO_2 in the atmosphere. Although, DOAS illustrated slight deviations at times, it gave a roughly accurate portrait of the atmospheric conditions of NO_2 occurring at night. The averaging done by DOAS heavily influences deviations between the two measurements. Although chemical and meteorological factors do play a role in deviating NO_2 mixing ratios in DOAS from the chemiluminescence, the primary influence is temporal and spatial averaging when NO_2 mixing ratios increase or decrease rapidly. The advantage of measuring over a long path length, which was done by DOAS, is for applications where large temporal and spatial scale averages are needed, such as intercomparisons with models. Selected models include grids that measure areas of long distances. For this reason, point measurements would not work as effectively as long path measurements. Another reason DOAS would be rendered useful is comparison of atmospheric concentrations with satellite measurements. Further work that can be done to enhance the accuracy of the DOAS instrument includes finding the exact concentration DOAS deviates from chemiluminescence. This can be done by calculating the concentration of other nitrogen species that form NO_2 as well as averaging deviations caused by temporal and spatial averaging as well as meteorology effects.

Appendix

Differential cross sections used:

Cross-section	Author, Date
NO_2	Vandaele, 1997
H_2O	Coheur, 2002
O_4	Hermans, 1999

Calculations:

Converting slant column density given by DOASIS to NO_2 concentrations

1. The slant column density is first divided by the total path length.

$$\frac{1.805x10^{17}}{22000\ cm} = 8.205\text{x}10^{12}$$

2. This value must then be corrected for the air mass factor by diving it by $2.49\text{x}10^{19}$

$$\frac{8.205x10^{12}}{2.49x10^{17}} = 3.29\ \text{x}10^{-5}$$

3. This value is then converted into a concentration by multiplying it with 10^6 to obtain the ppb value.

$$=3.29\text{x}10^{-5}\ \text{x}\ 10^6 = 32.95\ \text{ppb}$$

References

1. Barry, R.G. & Chorley R.J. Atmosphere, Weather and Climate.London, Menthuen & Co Ltd. 1971. p. 65

2. Halla, J.D. et al. Determination of Tropospheric Vertical Columns of NO_2 and Aerosol Optical Properties in a Rural Setting using MAX-DOAS. Atmospheric Chemistry and Physics. 2011. Vol. 11. p. 12475-12498.

3. McLaren, R. et al. NO_3 Radical Measurements in a Polluted Marine Environment: Links to Ozone Formation. Atmospheric Chemistry and Physics. 2010. Vol. 10. 4187-4206.

4. Ocak, S. Turalioglu, F. S. Effects of Meteorology on the Atmospheric Concentrations of Traffic Related Pollutants in Erzurum, Turkey. J. Int. Environmental Application & Science. 2008. Vol. 3 (5): 325-338.

5. Wojtal P. Noctural Measurements of HONO, NO_2 and NO_3 by Differential Optical Absorption Spectroscopy in Polluted Marine and Urban Atmospheres. 2013. p. 4-8

6. Platt, U.; Stutz, J. Physics of Earth and Space Environments. Differential Optical Absorption Spectroscopy Principles and Applications, Berlin, 2008; pp 23-32, 43-45.

7. Wojtal, P. et al. Pseudo Steady States of HONO measured in the Nocturnal Marine Boundary Layer: a Conceptual Model for HONO Formation on Aqueous Surfaces. Atmospheric Chemistry and Physics. 2011. Vol. 11. p. 3243-3261.

8. Yilmaz, S. Retrieval of Atmospheric Aerosol and Trace Gas Vertical Profiles using Multi-Axis Differential Optical Absorption Spectroscopy. 2012. p. 3-11